

DPBridge: Latent Diffusion Bridge for Dense Prediction

Haorui Ji Tao Jun Lin Hongdong Li
The Australian National University

{haorui.ji, taojun.lin, hongdong.li}@anu.edu.au

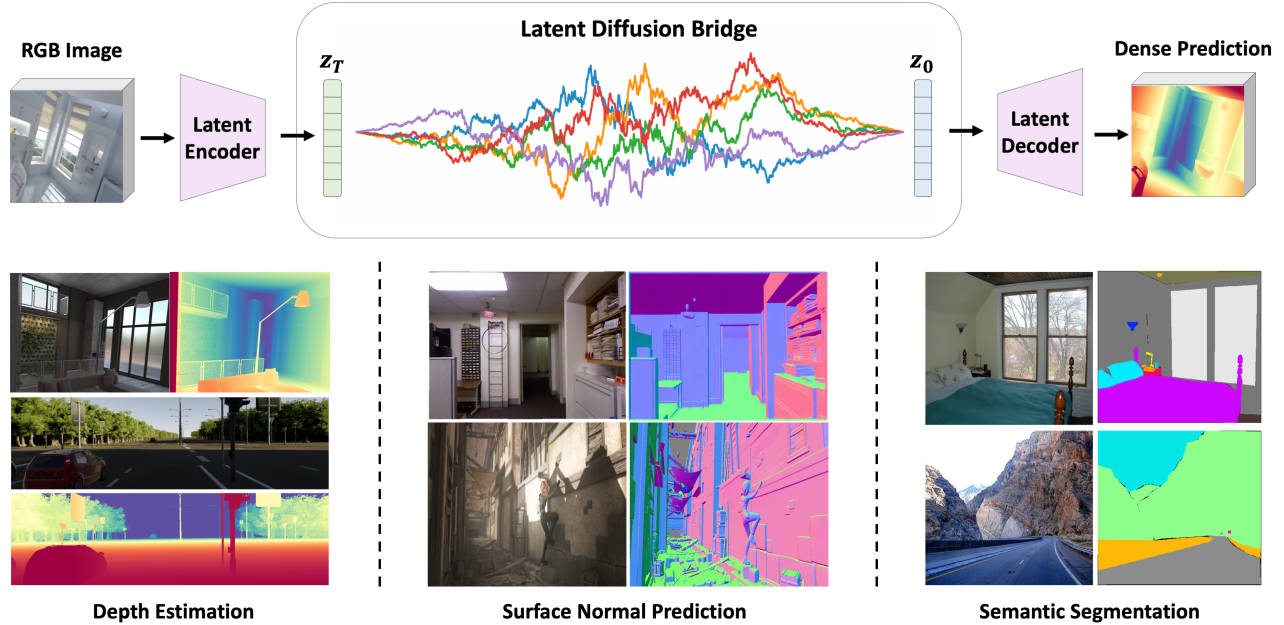


Figure 1. We present **DPBridge** to tackle general dense prediction tasks by establishing a stochastic transport between an RGB image and its corresponding dense map in the latent space based on a tractable diffusion bridge process. In addition, we introduce finetuning strategies to adapt large pretrained diffusion backbone to construct our bridge, leveraging its rich prior knowledge to enable both efficient training and robust generalization.

Abstract

Diffusion models have demonstrated remarkable success in dense prediction problems, which aims to model per-pixel relationship between RGB images and dense signal maps, thanks to their ability to effectively capture complex data distributions. However, initiating the reverse sampling trajectory from uninformative noise prior introduces limitations such as degraded performance and slow inference speed. In this work, we propose *DPBridge*, a generative framework that formulates dense prediction tasks as image-conditioned generation problems and establishes a direct mapping between input image and its corresponding dense map based on fully-tractable diffusion bridge process. This approach addresses aforementioned limitations in conventional diffusion-based solutions. In addition, we introduce finetuning strategies to adapt our model from pre-

trained image diffusion backbone, leveraging its rich visual prior knowledge to facilitate both efficient training and robust generalization ability. Experimental results shows that our *DPBridge* can achieve competitive performance compared to both feed-forward and diffusion-based approaches across various benchmarks, highlighting its effectiveness and adaptability.

1. Introduction

Diffusion models recently emerge as a family of powerful generative models that are able to capture complex data distributions through a sequence of forward and reverse processes [26, 46]. They accelerate the development of modern generative systems, and have consistently obtained state-of-the-art performance across various domains, such as image synthesis and video generation [17, 27, 46], controlled

editing [5, 50, 61], human pose estimation [28–30], inverse problem solving [11, 40, 53].

Despite such success, diffusion models still face limitations that hinder broader applications, especially in discriminative tasks like dense prediction. One major limitation stems from the fact that standard diffusion reverse process always starts from Gaussian noise, which contains little information about the target distribution. This will lead to degraded performance or prolonged convergence times. Current diffusion-based approaches formulate this type of tasks as image-conditioned generation problems and adopt measures like incorporating external conditions to the model [25, 47, 61], modifying the generation pipeline [41, 54], or adding extra guidance terms during sampling [11, 53] to deal with this issue. In this way they hope to better model the conditional generation process.

Instead of starting from noise, an feasible alternative is to leverage the inherent problem structure. Since the goal of dense prediction tasks is to model the probability transport between image and dense signal map distributions, it’s a rather straightforward idea to directly start the generative process from input RGB images, as they are structurally correlated to target signal maps and can naturally serve as more informative prior compared to noise. This motivates the exploration of a new family of computational frameworks, i.e. diffusion bridge models [36, 37, 39, 63]. They are based on a special type of diffusion process conditioned on given endpoints, thus enabling optimal transport between two distributions and generalizing beyond Gaussian priors.

Inspired by these intuition, we propose **Dense Prediction Bridge (DPBridge)**, a latent diffusion bridge model adapted from pretrained image diffusion backbone to handle general dense prediction tasks though the image-conditioned generation pipeline. In essence, we construct diffusion bridge process between the latent distributions of images and dense signal maps, with all intermediate samples along the trajectory being convex combinations of the paired data. The generative process thus becomes a series of transformations that iteratively synthesize desired signal maps starting from input images rather than pure noise, enabling faster inference speed as well as better generation quality.

In addition, to better adapt pretrained diffusion backbone to our DPBridge construction, we also propose novel finetuning strategies to allow for more effective knowledge transfer. In this way our model is augmented with rich visual prior knowledge, which not only helps boosting the perception performance as well as generalization capability, but also significantly speeds up training convergence. Fig.(1) is a high-level overview of DPBridge, while also demonstrating its effectiveness on three representative dense prediction tasks, i.e. depth estimation, surface nor-

mal prediction, and semantic segmentation, proving that our framework is theoretically universal and can be instantiated to different scenarios.

To summarize, our contributions are as follows:

- We propose DPBridge framework to deal with dense prediction tasks with generative pipeline by formulating them as instances of latent diffusion bridges.
- We propose finetuning strategies to effectively adapt large pretrained backbone to diffusion bridges, allowing for exploitation of visual prior knowledge and training efficiency improvements.
- Our proposed method exhibits competitive performance across different tasks in terms of both quantitative metrics and visual inspection, highlighting its effectiveness and generalization capability.

2. Related Works

2.1. Dense Prediction

Dense prediction refers to the type of problems whose outputs match the spatial dimensions of input data, often with the goal of assigning a value to each individual pixel. Typical examples include depth estimation, surface normal prediction, semantic segmentation, optical flow, etc. Common solutions can be categorized in discriminative and generative manner. Discriminative approaches focus on architecture design and introduce techniques like skip connections, dilated convolutions, multi-scale feature aggregation, and attention mechanisms [9, 34, 44] to better capture both local and global context for improved prediction accuracy. Generative methods, on the other hand, offer an alternative paradigm to tackle these problems through distribution modeling. Some works reuse or merge prior features from pretrained vision foundation models [4, 23, 62]. Others formulate these tasks as visual-condition guided generation process which refines the desired dense map iteratively [18, 24, 32].

2.2. Diffusion Bridge Models

Stochastic bridge models are a common tool in probability theory which describe the evolution of stochastic processes with given starting/ending points. When combined with diffusion models, they provide a new perspective to translate between different distributions and model conditional probabilities without the need for prior knowledge, therefore have been gaining increasing attention in the context of generative modeling in recent year [16, 38, 39]. They demonstrate the advantages of data-to-data generation paradigm over noise-to-data one on various tasks, including image-to-image translation [36, 37, 63], image restoration [13, 59], text-to-speech synthesis [10], etc. However, to the best of our knowledge, no prior work has explored leveraging diffusion bridge models on dense prediction tasks to facilitate

the distribution transport between images and dense signal maps, despite their intuitive structural closeness. Our work aims to fill in this research gap.

3. Preliminary

3.1. Diffusion Process

A diffusion process $\mathbb{Q} = \{\mathbf{z}_t \in \mathbb{R}^d : t \in [0, T]\}$ on space \mathbb{R}^d follows the stochastic differential equation of form

$$d\mathbf{z}_t = f(\mathbf{z}_t, t)dt + g(t)d\mathbf{w}_t \quad (1)$$

where \mathbf{w}_t is a standard Wiener process, $f : \mathbb{R}^d \times [0, T] \rightarrow \mathbb{R}$ and $g : [0, T] \rightarrow \mathbb{R}$ are the drift and diffusion coefficients that describe the evolution of this stochastic process. The transition kernel is specified as $q(\mathbf{z}_t|\mathbf{z}_0) = \mathcal{N}(\alpha_t\mathbf{z}_0, \sigma_t^2\mathbf{I})$ and the noise schedule comprising differentiable functions α_t, σ_t depends on the design choice of drift and diffusion coefficients. It is also common to assess the diffusion process in terms of the signal-to-noise ratio (SNR), defined as $\text{SNR}_t = \alpha_t^2/\sigma_t^2$.

3.2. Diffusion Bridge Process

Diffusion bridge process is a special type of diffusion process that guarantee to arrive at a prescribed final state T . One natural way of its construction is to derive the conditioned process from a reference diffusion process given terminal constraints. We can use Doob’s h-transform technique [42, 48] to modify a reference process \mathbb{Q} defined in Eqn.(1) to ensure that the event $\mathbf{z}_T = \mathbf{x}$ happens. Therefore the conditioned process $\mathbb{Q}^{\mathbf{x}}(\cdot) := \mathbb{Q}(\cdot|\mathbf{z}_T = \mathbf{x})$ follows the law of

$$d\mathbf{z}_t = [f(\mathbf{z}_t, t) + g^2(t)h(\mathbf{z}_t, t, \mathbf{x}, T)] dt + g(t)d\mathbf{w}_t \quad (2)$$

where $h(\mathbf{z}_t, t, \mathbf{x}, T) = \nabla_{\mathbf{z}_t} \log q(\mathbf{z}_T = \mathbf{x}|\mathbf{z}_t)$. Intuitively, the additional drift term $h(\mathbf{z}_t, t, \mathbf{x}, T)$ plays the role of steering \mathbf{z}_t towards the specified target point $\mathbf{z}_T = \mathbf{x}$, and it is ensured that $\mathbb{Q}^{\mathbf{x}}$ invariably passes \mathbf{x} at timestep T with probability 1 for any initial state \mathbf{z}_0 .

The transition kernel of $\mathbb{Q}^{\mathbf{x}}$, given by $q(\mathbf{z}_t|\mathbf{z}_0, \mathbf{z}_T)$, can be subsequently derived through Kolmogorov equation:

$$\begin{aligned} q(\mathbf{z}_t|\mathbf{z}_0, \mathbf{z}_T) &= \mathcal{N}(m_t\mathbf{z}_0 + n_t\mathbf{z}_T, \sigma_t^2\mathbf{I}) \\ m_t &= \alpha_t \left(1 - \frac{\text{SNR}_T}{\text{SNR}_t}\right) \\ n_t &= \frac{\text{SNR}_T}{\text{SNR}_t} \frac{\alpha_t}{\alpha_T} \\ \sigma_t &= \sigma_t \sqrt{1 - \frac{\text{SNR}_T}{\text{SNR}_t}}, \end{aligned} \quad (3)$$

where $\text{SNR}_t, \alpha_t, \sigma_t^2$ are all ingredients defined in the reference process \mathbb{Q} .

4. Method

4.1. Problem Formulation

We formulate different dense prediction tasks like depth estimation, surface normal prediction, semantic segmentation etc., as image-conditioned generation problems and propose DPBridge to model the conditional distributions $p(\mathbf{y}|\mathbf{x})$, where $\mathbf{y} \in \mathbb{R}^{H \times W \times C}$ indicates the desired dense signal map (e.g. segmentation, depth, surface normal), and $\mathbf{x} \in \mathbb{R}^{H \times W \times 3}$ is an RGB image. In the following sections, we’ll first introduce the motivation of utilizing diffusion bridge models to handle dense prediction problems. Then, we’ll elaborate the details of our proposed DPBridge framework, which is constructed based on pretrained diffusion backbone through proper finetuning.

4.2. Motivation: Bridge VS Diffusion

As introduced previously, the incompatibility that employ diffusion models to dense prediction task, which is essentially a image-conditioned generation problem, lies in its underlying iterative denoising process starting from Gaussian noise. In such cases, the distance between prior Gaussian distribution and data distribution remains large, requiring inevitably more sampling steps as well as ad-hoc conditioning mechanisms to converge to target distributions, at the risk of degraded performance and slow inference speed.

Bridge models, on the other hand, directly formulate generative processes as conditional probability paths. In this scenario, the boundary distribution is not restricted to Gaussian noise, but instead can be chosen as more informative priors, such as the condition data distribution. By establishing direct connections between different distributions, this formulation provides a more natural and efficient way to model probability transport compared with previous efforts. For example, it reduce the dependence on manually designed post-hoc guidance [11, 12, 53] or customized generation pipeline [41]. In addition, through implicitly integrates condition as part of the learned process, it provides a more flexible way to model intricacies between data and conditions without relying on explicit mechanisms like concatenation, attention [25, 47, 61], whose inductive bias may harm the overall performance when dealing with complex circumstances. Considering these advantages, we advocate that adopting diffusion bridge model will be a better fit to dense prediction tasks compared with conventional diffusion-based counterparts.

4.3. Dense Prediction Bridge

Given paired training data, a naive implementation is to construct the diffusion bridge model from scratch according to Sec.3.2. However, this approach is extremely resource-demanding, making it hard to implement with limited computation power. What’s more severe, it lacks the ability to

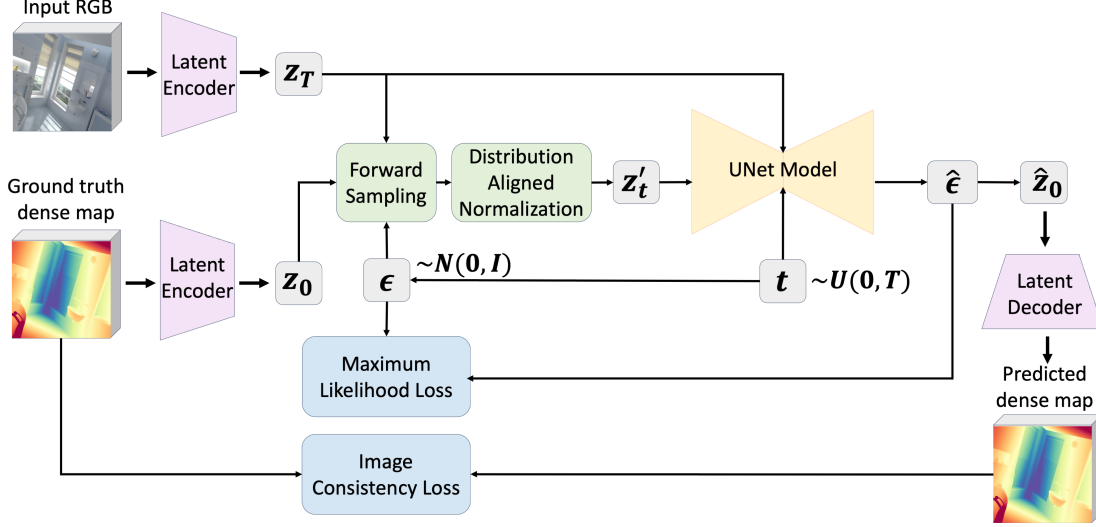


Figure 2. Overview of our training pipeline, which is conducted in the latent space based on diffusion bridge theory. To overcome the discrepancy with standard diffusion process and facilitate finetuning, we derive the maximum likelihood training objective of diffusion bridge process, propose a distribution aligned normalization strategy, and assist the training with an auxiliary image consistency loss.

harness rich scene understanding knowledge inherent in the vision foundation models, which have been proven significant in terms of boosting both perception quality and generalization performance in dense prediction tasks. Therefore, our DPBridge is build upon pretrained diffusion backbones through finetuning and we explore several strategies to handle the misalignment between original diffusion bridge process and standard diffusion process, aiming for more efficient knowledge transfer. Fig.2 gives an overview of the proposed finetuning pipeline, and we’ll explain the design of each component next.

4.4. Latent Space Implementation

Instead of directly learning in image pixel space, we follow common practices to perform diffusion steps in a compressed but perceptually aligned latent space, provided by an independently trained variational autoencoder (VAE). Specifically, both the target dense maps and RGB images are converted by the encoder to obtain $\mathbf{z}_0 = \mathcal{E}(\mathbf{y})$ and $\mathbf{z}_T = \mathcal{E}(\mathbf{x})$, serving as the boundary states. In this way the diffusion bridge process is henceforth learned in the latent space. To retrieve original signal map we can use the decoder to decode the predicted latents $\mathbf{y} = \mathcal{D}(\hat{\mathbf{z}}_0)$. In later part of this paper, with little abuse of notation, all derivations are conducted in the latent space.

4.5. Training Objective

4.5.1 Maximum Likelihood Loss

In previous diffusion bridge models, widely-used techniques for learning the reverse process that corresponds to Eqn.(2) is to follow the theory of [1], use a neural network to approximate the score function and apply score match-

ing technique. We notice that analytical form of diffusion bridge’s reverse transition kernel is directly obtainable, therefore the usage of maximum likelihood training can also be applied, which is performed by optimizing the Evidence Lower Bound (ELBO). It yields a more stable loss function compared with score matching and better aligns with the pretrained backbone. Given the fixed terminal state \mathbf{z}_T , the expectation of data log-likelihood possesses the following ELBO formulation:

$$\text{ELBO} = \mathbb{E}_{p(\mathbf{z}_0)} \left[\mathbb{E}_{p(\mathbf{z}_1|\mathbf{z}_0)} [\log p_\theta(\mathbf{z}_0 | \mathbf{z}_1, \mathbf{z}_T)] - \sum_{t=2}^T \mathbb{E}_{p(\mathbf{z}_t|\mathbf{z}_0)} [\mathbb{D}_{KL}(q(\mathbf{z}_{t-1} | \mathbf{z}_0, \mathbf{z}_t, \mathbf{z}_T) || p_\theta(\mathbf{z}_{t-1} | \mathbf{z}_t, \mathbf{z}_T))] \right] \quad (4)$$

where $q(\mathbf{z}_{t-1}|\mathbf{z}_t, \mathbf{z}_0, \mathbf{z}_T)$ and $p_\theta(\mathbf{z}_{t-1}|\mathbf{z}_t, \mathbf{z}_T)$ are the transition kernel of true reverse process and our modeled generative process and \mathbb{D}_{KL} is the KL divergence. Utilize Bayes’ theorem and Markov chain property, we obtain:

$$q(\mathbf{z}_{t-1}|\mathbf{z}_t, \mathbf{z}_0, \mathbf{z}_T) = \frac{q(\mathbf{z}_t|\mathbf{z}_{t-1}, \mathbf{z}_T)q(\mathbf{z}_{t-1}|\mathbf{z}_0, \mathbf{z}_T)}{q(\mathbf{z}_t|\mathbf{z}_0, \mathbf{z}_T)} = \mathcal{N}(\tilde{\boldsymbol{\mu}}_t(\mathbf{z}_t, \mathbf{z}_0, \mathbf{z}_T), \tilde{\boldsymbol{\sigma}}_t^2 \mathbf{I}) \quad (5)$$

For simplicity, we define the following notations: $a_t = m_t/m_{t-1}$, $b_t = n_t - a_t \cdot n_{t-1}$, $\delta_t^2 = \sigma_t^2 - a_t^2 \cdot \sigma_{t-1}^2$. The mean value term is:

$$\begin{aligned} \tilde{\boldsymbol{\mu}}_t(\mathbf{z}_t, \mathbf{z}_0, \mathbf{z}_T) &= k_1 \mathbf{z}_t + k_2 \mathbf{z}_0 + k_3 \mathbf{z}_T \\ k_1 &= \frac{\sigma_{t-1}^2}{\sigma_t^2} \cdot a_t \\ k_2 &= \frac{\delta_t^2}{\sigma_t^2} \cdot m_{t-1} \\ k_3 &= \frac{\delta_t^2}{\sigma_t^2} \cdot n_{t-1} - \frac{\sigma_{t-1}^2}{\sigma_t^2} \cdot a_t \cdot b_t, \end{aligned} \quad (6)$$

and the variance is:

$$\tilde{\sigma}_t^2 = \frac{\sigma_{t-1}^2}{\sigma_t^2} \cdot \delta_t^2 \quad (7)$$

Assume $p_\theta(\mathbf{z}_{t-1}|\mathbf{z}_t, \mathbf{z}_T)$ is also a Gaussian distribution parameterized as $\mathcal{N}(\boldsymbol{\mu}_\theta(\mathbf{z}_t, \mathbf{z}_T, t), \boldsymbol{\Sigma}_\theta(\mathbf{z}_t, \mathbf{z}_T, t))$ and let $\boldsymbol{\Sigma}_\theta(\mathbf{z}_t, \mathbf{z}_T, t) = \tilde{\sigma}_t^2$ for derivation simplicity, maximizing the ELBO is equivalent to minimizing:

$$\mathcal{L}_{elbo} = \mathbb{E}_{t, \mathbf{z}_0, \mathbf{z}_t, \mathbf{z}_T} \left[\frac{1}{2\tilde{\sigma}_t^2} \|\tilde{\boldsymbol{\mu}}_t - \boldsymbol{\mu}_\theta(\mathbf{z}_t, \mathbf{z}_T, t)\|^2 \right] \quad (8)$$

Similar to the strategy in DDPM [26], we use a network $\epsilon_\theta(\mathbf{z}_t, \mathbf{z}_T, t)$ to parameterize noise instead of posterior mean and further simplified the loss as:

$$\mathcal{L}_{elbo} = \mathbb{E}_{t, \mathbf{z}_0, \mathbf{z}_t, \mathbf{z}_T} \left[\|\epsilon - \epsilon_\theta(\mathbf{z}_t, \mathbf{z}_T, t)\|^2 \right], \quad (9)$$

4.5.2 Image Consistency Loss

In addition to the common likelihood loss evaluated in the latent space, we also incorporate an image-level consistency loss, where we first convert the latent prediction back to image space, and then evaluate its consistency with the ground truth dense map using a simple MSE loss.

$$\mathcal{L}_{ic} = \|\mathcal{D}(\hat{\mathbf{z}}_0) - \mathbf{y}\|^2 \quad (10)$$

The reason is that the compression of input data in the latent space will lead to a loss of high-frequency information, harming the model’s ability of preserving fine-grained spatial details. By introducing an auxiliary loss at image level, we ensure that the model is capable of retaining spatial information which is essential for precise per-pixel prediction. This dual loss strategy leverages the compactness of latent space for efficiency while still anchoring the training process to the fidelity of full-resolution dense map prediction, thus leading to performance improvement. Combined these two losses together, our final training objective becomes:

$$\mathcal{L} = \omega_1 \mathcal{L}_{elbo} + \omega_2 \mathcal{L}_{ic} \quad (11)$$

where ω_1, ω_2 are adjustable hyperparameters to balance the loss. An overview of DPBridge’s training pipeline shown in Algorithm.1.

4.6. Distribution Alignment Normalization

A notable challenge during finetuning is the misalignment of intermediate sample’s marginal distribution $q(\mathbf{z}_t)$ between DPBridge and diffusion backbone, due to the difference in the forward transition kernel. This misalignment will weaken the model’s inherent denoising ability, thus limiting the effectiveness of knowledge transfer. To address

Algorithm 1 Training

Require: Encoder \mathcal{E} ; Decoder \mathcal{D} ; Loss weights ω_1, ω_2

- 1: **repeat**
 - 2: Retrieve paired data (\mathbf{x}, \mathbf{y})
 - 3: $\mathbf{z}_0 = \mathcal{E}(\mathbf{y}), \mathbf{z}_T = \mathcal{E}(\mathbf{x})$
 - 4: $t \sim \text{Uniform}(\{1, \dots, T\}), \epsilon \sim \mathcal{N}(\mathbf{0}, \mathbf{I})$
 - 5: $\mathbf{z}_t = n_t \mathbf{z}_T + m_t \mathbf{z}_0 + \sigma_t \epsilon$
 - 6: $\mathbf{z}'_t = \frac{1}{\sqrt{n_t^2 + \sigma_t^2}} (\mathbf{z}_t - n_t \mathbf{z}_T)$
 - 7: $\mathcal{L}_{elbo} = \|\epsilon - \epsilon_\theta(\mathbf{z}'_t, \mathbf{z}_T, t)\|^2$,
 - 8: $\hat{\mathbf{z}}_0 = \frac{1}{m_t} (\mathbf{z}_t - n_t \mathbf{z}_T - \sigma_t \epsilon_\theta(\mathbf{z}'_t, \mathbf{z}_T, t))$
 - 9: $\mathcal{L}_{ic} = \|\mathcal{D}(\hat{\mathbf{z}}_0) - \mathbf{y}\|^2$
 - 10: Take gradient step on $\nabla_\theta (\omega_1 \mathcal{L}_{elbo} + \omega_2 \mathcal{L}_{ic})$
 - 11: **until** converged
-

Algorithm 2 Inference

Require: Encoder \mathcal{E} ; Decoder \mathcal{D} ; Trained $\epsilon_\theta(\cdot, \cdot, \cdot)$

- 1: $\mathbf{z}_T = \mathcal{E}(\mathbf{x})$
 - 2: **for** $t = T, \dots, 1$ **do**
 - 3: $\epsilon \sim \mathcal{N}(\mathbf{0}, \mathbf{I})$ if $t > 1$, else $\epsilon = \mathbf{0}$
 - 4: $\mathbf{z}'_t = \frac{1}{\sqrt{n_t^2 + \sigma_t^2}} (\mathbf{z}_t - n_t \mathbf{z}_T)$
 - 5: $\hat{\mathbf{z}}_0 = \frac{1}{m_t} (\mathbf{z}_t - n_t \mathbf{z}_T - \sigma_t \epsilon_\theta(\mathbf{z}'_t, \mathbf{z}_T, t))$
 - 6: $\mathbf{z}_{t-1} = k_1 \mathbf{z}_t + k_2 \hat{\mathbf{z}}_0 + k_3 \mathbf{z}_T + \tilde{\sigma}_t \epsilon$
 - 7: **end for**
 - 8: $\mathbf{y} = \mathcal{D}(\hat{\mathbf{z}}_0)$
 - 9: **return** \mathbf{y}
-

this issue, we propose a distribution alignment normalization technique to fill in the gap between the two distributions. Specifically, we normalize the intermediate latents computed from Eqn.(3) to match the form of a standard diffusion process:

$$\mathbf{z}'_t = \frac{\mathbf{z}_t - m_t \mathbf{z}_T}{\sqrt{n_t^2 + \sigma_t^2}} = \frac{n_t}{\sqrt{n_t^2 + \sigma_t^2}} \mathbf{z}_0 + \frac{\sigma_t}{\sqrt{n_t^2 + \sigma_t^2}} \epsilon_t \quad (12)$$

Since the square sum of coefficients is equal to 1, the normalized bridge process $\{\mathbf{z}'_t : t \in [0, T]\}$ is the same as a standard VP process, making the marginal distribution of these two aligned. Therefore by feeding the normalized sample \mathbf{z}'_t in the network ϵ_θ , we can fully exploit the denoising capability from pretrained diffusion backbone.

4.7. Network Architecture

To better utilize visual information (\mathbf{z}_T in our case), we concatenating both intermediate and terminal state samples along the feature dimension and send in the noise prediction network as a whole. To address the dimension incompatibility with pretrained backbone, the input channels of the network are thus doubled to accommodate the concatenated input. In addition, as suggested by [32], we duplicate the weight tensor of these accommodated layers and divide the

values by two to preserve the input magnitude to subsequent layers. As DPBridge is an image-conditioned generative framework, we employ null-text embedding for all cross-attention layers to eliminate the impact of text prompts.

4.8. Accelerate Inference

Similar to the idea of DDIM [52], the inference process of DPBridge can be accelerated by utilizing a non-Markovian process while maintaining the same marginal distributions for all intermediate samples along the sampling path. Specifically, we can sample on a subset of timesteps $\{t_i\}_{i=1}^N$, where $0 = t_0 < t_1 < \dots < t_{N-1} < t_N = T$ and the number of sampling steps N can be set independently from the original timesteps T on which the bridge model is trained. The accelerated inference process can be thus described as:

$$\mathbf{z}_{t_n} = n_{t_n} \mathbf{z}_T + m_{t_n} \hat{\mathbf{z}}_0 + \sqrt{\sigma_{t_n}^2 - g_n^2} \frac{\mathbf{z}_{t_{n+1}} - n_{t_{n+1}} \mathbf{z}_T - m_{t_{n+1}} \hat{\mathbf{z}}_0}{\sigma_{t_{n+1}}} + g_n \epsilon \quad (13)$$

where g_n is the variance parameter that controls the stochasticity behavior of the reverse sampling process. We note that when $g_n = \hat{\sigma}_t^2$ which is calculated from Eqn.(5), the process becomes a Markovian bridge. The basic inference process of DPBridge is summarized in Algorithm.2. If adopt acceleration, one can utilize Eqn.(13) during implementation.

5. Experiments

We evaluate the proposed DPBridge approach mainly on two representative dense prediction tasks, i.e., depth estimation and surface normal prediction. We'll start by a brief introduction of experiment settings of these two tasks, followed by quantitative and qualitative analysis. Lastly, we conduct detailed ablation studies and investigate the influence each design component respectively.

5.1. Experiments Setup

Datasets. The basic setting for depth estimation and surface normal prediction experiments are similar. We use two synthetic datasets, HyperSim [45] and Virtual KITTI [8], which cover both indoor and outdoor scenes, for training. To comprehensively evaluate the model performance and demonstrate its generalization capability, we conduct zero-shot evaluations on real-world datasets. For depth estimation, this includes NYUv2 [51], KITTI [22], ScanNet [15], ETH3D [49] and DIODE [56]. For surface normal prediction, we additionally incorporate iBims [33] and Sintel [7] datasets in the evaluation pipeline. For fair comparison, we use the same validation split as in previous methods [32].

Evaluation Metrics. For depth estimation, we follow the affine-invariant evaluation protocol, where we first align

the prediction results to the ground truth with least squares fitting, and then use Absolute Mean Relative Error (AbsRel) and δ_1 accuracy to assess the performance. Denote the ground truth depth \mathbf{d} , predicted depth $\hat{\mathbf{d}}$, and the number of valid pixels N , the AbsRel is calculated as $\frac{1}{N} \sum_{i=1}^N \|\mathbf{d}_i - \hat{\mathbf{d}}_i\|/\mathbf{d}_i$, and δ_1 accuracy is measured using the ratio of pixels satisfying $\max(\mathbf{d}_i/\hat{\mathbf{d}}_i, \hat{\mathbf{d}}_i/\mathbf{d}_i) < 1.25$. For the metrics of surface normal task, we report the commonly used mean angular error between the ground-truth normal vectors and the prediction results, as well as the percentage of pixels with an angular error below 11.25 degrees.

5.2. Implementation Details

We implement DPBridge based on Stable Diffusion (SD) v1.5 [46] as backbone. During training, the number of timesteps of is set to be 1000, and we use 50 sampling steps during inference with considerations of both quality and efficiency. Training our method takes 30K iterations using the Adam optimizer with a base learning rate of 3×10^{-5} and an exponential decay strategy after 100-step warm-up. The batch size is 2, but with 8 steps gradient accumulation, the effective batch size is equivalent to 16. We also apply random horizontal flipping augmentation during training. The whole process takes approximately 2 days to complete on a single Nvidia RTX 3090Ti GPU.

5.3. Quantitative and Qualitative Results

Tab.1 and Tab.2 summarize the quantitative metrics of DPBridge compared with diffusion-based and bridge-based counterparts, who are most closely related to our work. The reason we use SDv1.5 instead of more advanced SDv2.1 as backbone is that our current pipeline does not support v-prediction parameterization as in SDv2.1, and this incompatibility will undermine the model's knowledge transfer ability. We'll present more detail analysis in the ablation study. For a fair comparison, we re-implement all baseline methods using the same SDv1.5 backbone as we do, and report the results. We also conduct comparison with feed-forward and diffusion-based approaches based on SDv2.1 backbone, and the complete results is presented in the Appendix. DPBridge outperforms most methods in our evaluation setting and even be comparable with state-of-the-art that is trained with SDv2.1. Specifically, when compared with bridge models like I2SB and BBDM that are trained from scratch, we exceed their performance by a large margin, justifying our proposal that adapting prior knowledge to bridge process indeed benefits the perception performance. In terms of diffusion-based methods, DPBridge can also achieve the best result, showcasing that adopting bridge process to handle dense prediction tasks is indeed advantageous over standard diffusion framework.

The qualitative results for depth estimation is conducted on KITTI and ETH3D datasets, as shown in Fig. 3. We can

Method	Model Type		NYUv2		KITTI		ETH3D		ScanNet		DIODE	
	DM	BM	AbsRel↓	δ_1 ↑	AbsRel↓	δ_1 ↑	AbsRel↓	δ_1 ↑	AbsRel↓	δ_1 ↑	AbsRel↓	δ_1 ↑
Marigold [32]	✓		8.6	93.6	<u>13.8</u>	<u>82.6</u>	9.3	<u>93.2</u>	10.4	89.7	33.6	<u>73.9</u>
Geowizard [20]	✓		8.5	93.7	16.2	75.6	<u>9.1</u>	93.1	<u>9.0</u>	<u>93.0</u>	<u>32.0</u>	72.2
E2E-FT [21]	✓		<u>8.2</u>	<u>94.0</u>	15.4	77.9	10.6	89.8	9.2	92.3	32.9	73.7
ControlNet [61]	✓		45.5	54.6	55.2	40.2	30.5	58.8	25.7	68.3	52.1	50.1
InstructPix2Pix [6]	✓		35.2	60.0	47.7	51.2	26.1	66.7	21.4	75.3	44.8	58.0
I2SB [37]		✓	24.9	73.4	37.7	57.9	40.6	52.0	21.2	66.1	40.2	59.1
BBDM [36]		✓	27.9	65.5	47.2	45.1	46.4	48.8	22.7	67.0	34.6	64.7
DPBridge (Ours)		✓	6.9	95.7	11.2	87.3	8.1	93.2	7.5	94.7	29.7	78.6

Table 1. Quantitative comparison of DPBridge with state-of-the-art affine-invariant depth estimation methods on zero-shot benchmarks. All metrics are presented in percentage terms with best and second-best results marked by **bold** and underline. DM and BM correspond to diffusion models and bridge models respectively. All models are trained using SDv1.5 as backbone.

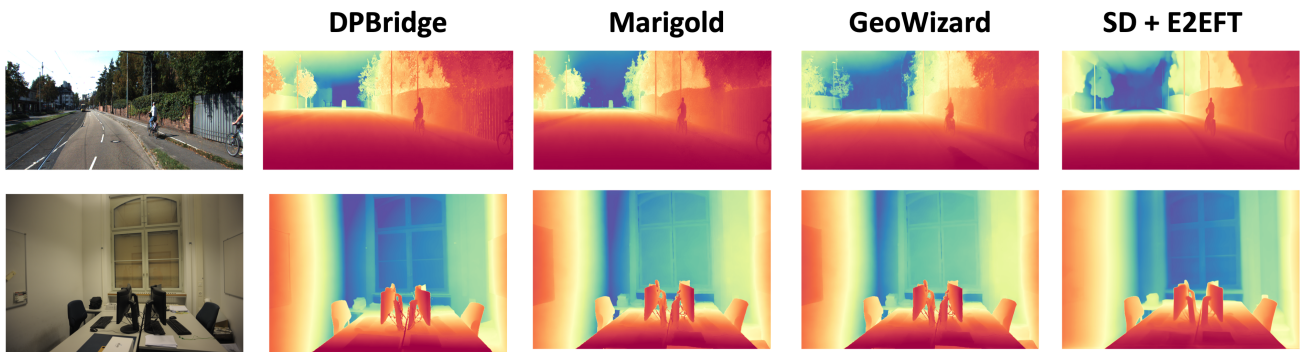


Figure 3. Qualitative comparison of monocular depth estimation methods on KITTI and ETH3D dataset. DPBridge is able to generalize in both indoor and outdoor scenes, successively capturing fine-grained details such as leaves and structures on the fence (KITTI).

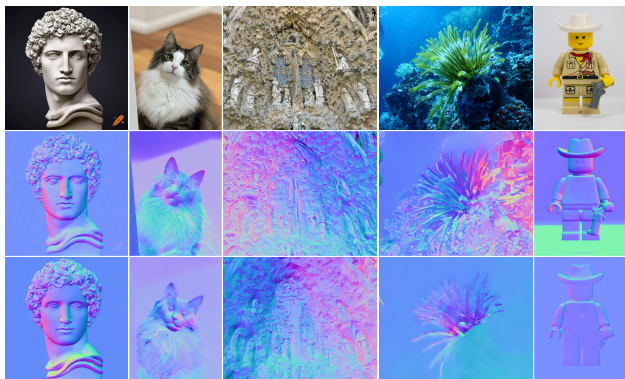


Figure 4. Qualitative comparison between our (above) and Marigold trained on SDv1.5 (below) on normal estimation results, DPBridge is able to capture more textures from the photos in-the-wild.

see that E2E-FT tends to produce blurry and smooth predictions, while Geowizard fails to provide accurate estimation in relatively long distance range. In contrast, DPBridge

perform well in both indoor and outdoor scenes, capturing fine-level details in both near and faraway regions, like the contour of leaves, fences, cars, computers or windows. We also present visualizations on in-the-wild images for surface normal prediction task. DPBridge is able to predict high-quality surface normals equipped with fine-grained textures. This strong generalization capability can be attribute to that we effectively harness extensive visual prior knowledge inherent in the pretrained diffusion backbone.

Method	NYUv2		ScanNet		iBims-1		Sintel	
	Mean↓	11.25° ↑						
Marigold [32]	22.3	40.0	23.3	37.6	28.0	38.5	52.1	8.1
Geowizard [20]	21.7	44.2	22.0	42.1	28.2	37.9	45.8	11.0
E2E-FT [21]	17.7	57.8	17.4	57.4	18.0	64.6	43.9	14.1
DPBridge (Ours)	<u>18.1</u>	<u>54.2</u>	<u>18.0</u>	<u>54.5</u>	<u>24.3</u>	<u>51.2</u>	41.2	19.4

Table 2. Quantitative comparison of DPBridge with state-of-the-art surface normal prediction methods on zero-shot benchmarks. All metrics are presented in percentage terms with best and second-best results marked by **bold** and underline. DM and BM correspond to diffusion models and bridge models respectively. All models are trained using SDv1.5 as backbone.

Design Components			NYUv2		KITTI	
<i>FT</i>	<i>DAN</i>	<i>IC</i>	AbsRel↓	δ_1 ↑	AbsRel↓	δ_1 ↑
	✓	✓	26.8	85.7	33.6	57.7
✓			8.8	93.0	14.0	83.1
✓		✓	8.5	93.3	13.4	83.9
✓	✓		7.5	94.9	13.1	84.6
✓	✓	✓	6.9	95.7	11.2	87.3

Table 3. The ablation study regarding the design components of DPBridge. *FT* stands for utilizing pretrained diffusion backbone during training. *DAN* denotes distribution aligned normalization technique. *IC* indicates image consistency loss.

Parameterization			Backbone		Steps	NYUv2		KITTI	
<i>Noise</i>	<i>Sample</i>	<i>Velocity</i>	v1.5	v2		AbsRel↓	δ_1 ↑	AbsRel↓	δ_1 ↑
	✓		✓		50	8.2	94.5	12.7	85.0
		✓	✓		50	23.7	59.1	30.5	56.7
✓				✓	50	7.6	95.6	12.0	85.8
	✓			✓	50	7.7	94.6	12.4	85.2
		✓		✓	50	22.8	62.4	28.5	60.1
✓			✓		5	12.1	86.5	19.4	66.5
✓			✓		10	7.7	95.1	12.5	84.1
✓			✓		50	6.9	95.7	11.2	87.3
✓			✓		100	6.8	95.1	11.4	87.5
✓			✓		200	6.6	95.6	12.3	84.8

Table 4. The ablation study regarding the hyperparameter choice of diffusion bridge process. Options include different network parameterizations, the version of SD to use as backbone, and the number of denoising steps during inference.

5.4. Ablation Studies

To evaluate the effectiveness of each design component and training setting, we conduct ablation studies using depth estimation tasks on the NYUv2 and KITTI datasets. The results are summarized in Tab.3 and Tab.4, with detailed discussions provided below.

5.4.1 Design Components

Finetuning VS Training From Scratch. To assess whether adapting pretrained diffusion backbones to our DPBridge improves perception performance, we compare the difference between finetuning and training from scratch paradigm. As shown in the first row of Tab.3, fine-tuning significantly outperforms training from scratch under identical experimental settings. This difference is due to two factors: first, foundation models trained on large, diverse datasets capture universal visual priors, aiding knowledge transfer to dense prediction tasks. Second, training from scratch requires more iterations for convergence. These observations suggest that building DPBridge on pretrained backbones is indeed advantageous.

Distribution Alignment Normalization. Next, we evaluate whether aligning the marginal distributions between diffusion bridge process and standard diffusion process is ben-

eficial. As shown in the second and fourth rows of Tab.3, incorporating a distribution alignment normalization step before inputting data into the noise prediction network noticeably improves performance.

Image Consistency Loss. Regarding the auxiliary image consistency loss, the comparison between the third and fourth rows in Tab.3 shows that while effective, its impact is less significant than that of distribution alignment normalization. This is probably because it primarily influences regions where masked and valid areas overlap, which constitute only a relatively small proportion of the data. However, when integrated with other design components, the overall performance is significantly improved.

5.4.2 Bridge Process Hyperparameters

Parameterization and Backbone Selection. Apart from the noise prediction scheme used in our main experiments, we also consider how the choice of parameterization combined with the backbone selection influences performance. Results in Tab.4 reveal two key findings: (1) v-parameterization performs significantly worse compared with other two options, highlighting the need for further research on deriving objectives specific to the diffusion bridge process, and (2) "noise prediction + SDv1.5" achieves the best results, indicating that the parameterization during finetuning should align with that of the backbone to maximize knowledge transfer efficiency.

Number of Sampling Steps. We evaluate performance with varying numbers of sampling steps during inference. As shown in the lower part of Tab.4, increasing sampling steps initially improves perception performance rapidly before leveling off. Notably, compared to the results in Tab.1, where all other diffusion-based methods are evaluated with 50 steps setting, DPBridge achieves comparable performance with fewer steps, demonstrating the efficiency of our proposed method.

6. Conclusion

In this paper, we present DPBridge, a latent diffusion bridge model to tackle general dense prediction tasks. We establish a direct mapping between input RGB images and their corresponding dense maps in the latent space based on fully-tractable diffusion bridge process. In this way, the prior distribution is no longer constrained to uninformative noise, but instead can be chosen as more structurally correlated ones. In addition, we introduce effective finetuning strategies to adapt large pretrained diffusion backbone to our bridge model construction, leveraging its rich prior knowledge to boost training speed and achieve remarkable perception performance. Future research directions include deriving v-prediction parameterization of diffusion bridge process, and extending to other dense prediction tasks.

References

- [1] Brian DO Anderson. Reverse-time diffusion equation models. *Stochastic Processes and their Applications*, 12(3):313–326, 1982. 4
- [2] Gwangbin Bae and Andrew J Davison. Rethinking inductive biases for surface normal estimation. In *Proceedings of the IEEE/CVF Conference on Computer Vision and Pattern Recognition*, pages 9535–9545, 2024. 3
- [3] Gwangbin Bae, Ignas Budvytis, and Roberto Cipolla. Estimating and exploiting the aleatoric uncertainty in surface normal estimation. In *Proceedings of the IEEE/CVF International Conference on Computer Vision*, pages 13137–13146, 2021. 3
- [4] Dmitry Baranchuk, Ivan Rubachev, Andrey Voynov, Valentin Khrukov, and Artem Babenko. Label-efficient semantic segmentation with diffusion models. *arXiv preprint arXiv:2112.03126*, 2021. 2
- [5] Georgios Batzolis, Jan Stanczuk, Carola-Bibiane Schönlieb, and Christian Etmann. Conditional image generation with score-based diffusion models. *arXiv preprint arXiv:2111.13606*, 2021. 2
- [6] Tim Brooks, Aleksander Holynski, and Alexei A Efros. Instructpix2pix: Learning to follow image editing instructions. In *Proceedings of the IEEE/CVF Conference on Computer Vision and Pattern Recognition*, pages 18392–18402, 2023. 7, 3
- [7] Daniel J Butler, Jonas Wulff, Garrett B Stanley, and Michael J Black. A naturalistic open source movie for optical flow evaluation. In *Computer Vision—ECCV 2012: 12th European Conference on Computer Vision, Florence, Italy, October 7–13, 2012, Proceedings, Part VI 12*, pages 611–625. Springer, 2012. 6, 7
- [8] Johann Cabon, Naila Murray, and Martin Humenberger. Virtual kitti 2. *arXiv preprint arXiv:2001.10773*, 2020. 6
- [9] Liang-Chieh Chen. Rethinking atrous convolution for semantic image segmentation. *arXiv preprint arXiv:1706.05587*, 2017. 2
- [10] Zehua Chen, Guande He, Kaiwen Zheng, Xu Tan, and Jun Zhu. Schrodinger bridges beat diffusion models on text-to-speech synthesis. *arXiv preprint arXiv:2312.03491*, 2023. 2
- [11] Hyungjin Chung, Jeongsol Kim, Michael T Mccann, Marc L Klasky, and Jong Chul Ye. Diffusion posterior sampling for general noisy inverse problems. *arXiv preprint arXiv:2209.14687*, 2022. 2, 3
- [12] Hyungjin Chung, Byeongsu Sim, Dohoon Ryu, and Jong Chul Ye. Improving diffusion models for inverse problems using manifold constraints. *Advances in Neural Information Processing Systems*, 35:25683–25696, 2022. 3
- [13] Hyungjin Chung, Jeongsol Kim, and Jong Chul Ye. Direct diffusion bridge using data consistency for inverse problems. *Advances in Neural Information Processing Systems*, 36, 2024. 2
- [14] Marius Cordts, Mohamed Omran, Sebastian Ramos, Timo Rehfeld, Markus Enzweiler, Rodrigo Benenson, Uwe Franke, Stefan Roth, and Bernt Schiele. The cityscapes dataset for semantic urban scene understanding. In *Proceedings of the IEEE conference on computer vision and pattern recognition*, pages 3213–3223, 2016. 5
- [15] Angela Dai, Angel X Chang, Manolis Savva, Maciej Halber, Thomas Funkhouser, and Matthias Nießner. Scannet: Richly-annotated 3d reconstructions of indoor scenes. In *Proceedings of the IEEE conference on computer vision and pattern recognition*, pages 5828–5839, 2017. 6
- [16] Valentin De Bortoli, James Thornton, Jeremy Heng, and Arnaud Doucet. Diffusion schrödinger bridge with applications to score-based generative modeling. *Advances in Neural Information Processing Systems*, 34:17695–17709, 2021. 2
- [17] Prafulla Dhariwal and Alexander Nichol. Diffusion models beat gans on image synthesis. *Advances in neural information processing systems*, 34:8780–8794, 2021. 1
- [18] Yiqun Duan, Xianda Guo, and Zheng Zhu. Diffusiondepth: Diffusion denoising approach for monocular depth estimation. *arXiv preprint arXiv:2303.05021*, 3, 2023. 2
- [19] Ainaz Eftekhari, Alexander Sax, Jitendra Malik, and Amir Zamir. Omnidata: A scalable pipeline for making multi-task mid-level vision datasets from 3d scans. In *Proceedings of the IEEE/CVF International Conference on Computer Vision*, pages 10786–10796, 2021. 3
- [20] Xiao Fu, Wei Yin, Mu Hu, Kaixuan Wang, Yuexin Ma, Ping Tan, Shaojie Shen, Dahua Lin, and Xiaoxiao Long. Geowizard: Unleashing the diffusion priors for 3d geometry estimation from a single image. In *European Conference on Computer Vision*, pages 241–258. Springer, 2025. 7, 3
- [21] Gonzalo Martin Garcia, Karim Abou Zeid, Christian Schmidt, Daan de Geus, Alexander Hermans, and Bastian Leibe. Fine-tuning image-conditional diffusion models is easier than you think. *arXiv preprint arXiv:2409.11355*, 2024. 7, 3
- [22] Andreas Geiger, Philip Lenz, and Raquel Urtasun. Are we ready for autonomous driving? the kitti vision benchmark suite. In *2012 IEEE conference on computer vision and pattern recognition*, pages 3354–3361. IEEE, 2012. 6
- [23] Rui Gong, Martin Danelljan, Han Sun, Julio Delgado Mangas, and Luc Van Gool. Prompting diffusion representations for cross-domain semantic segmentation. *arXiv preprint arXiv:2307.02138*, 2023. 2
- [24] Ming Gui, Johannes S Fischer, Ulrich Prestel, Pingchuan Ma, Dmytro Kotovenko, Olga Grebenkova, Stefan Andreas Baumann, Vincent Tao Hu, and Björn Ommer. Depthfm: Fast monocular depth estimation with flow matching. *arXiv preprint arXiv:2403.13788*, 2024. 2, 3
- [25] Jonathan Ho and Tim Salimans. Classifier-free diffusion guidance. *arXiv preprint arXiv:2207.12598*, 2022. 2, 3
- [26] Jonathan Ho, Ajay Jain, and Pieter Abbeel. Denoising diffusion probabilistic models. *Advances in neural information processing systems*, 33:6840–6851, 2020. 1, 5
- [27] Jonathan Ho, Tim Salimans, Alexey Gritsenko, William Chan, Mohammad Norouzi, and David J Fleet. Video diffusion models. *arXiv:2204.03458*, 2022. 1
- [28] Haorui Ji and Hongdong Li. 3d human pose analysis via diffusion synthesis. *arXiv preprint arXiv:2401.08930*, 2024. 2

- [29] Haorui Ji, Hui Deng, Yuchao Dai, and Hongdong Li. Unsupervised 3d pose estimation with non-rigid structure-from-motion modeling. In *Proceedings of the IEEE/CVF Winter Conference on Applications of Computer Vision*, pages 3314–3323, 2024.
- [30] Zhongyu Jiang, Zhuoran Zhou, Lei Li, Wenhao Chai, Cheng-Yen Yang, and Jenq-Neng Hwang. Back to optimization: Diffusion-based zero-shot 3d human pose estimation. In *Proceedings of the IEEE/CVF Winter Conference on Applications of Computer Vision*, pages 6142–6152, 2024. 2
- [31] Oğuzhan Fatih Kar, Teresa Yeo, Andrei Atanov, and Amir Zamir. 3d common corruptions and data augmentation. In *Proceedings of the IEEE/CVF Conference on Computer Vision and Pattern Recognition*, pages 18963–18974, 2022. 3
- [32] Bingxin Ke, Anton Obukhov, Shengyu Huang, Nando Metzger, Rodrigo Caye Daudt, and Konrad Schindler. Repurposing diffusion-based image generators for monocular depth estimation. In *Proceedings of the IEEE/CVF Conference on Computer Vision and Pattern Recognition*, pages 9492–9502, 2024. 2, 5, 6, 7, 3
- [33] Tobias Koch, Lukas Liebel, Friedrich Fraundorfer, and Marco Korner. Evaluation of cnn-based single-image depth estimation methods. In *Proceedings of the European Conference on Computer Vision (ECCV) Workshops*, pages 0–0, 2018. 6
- [34] Katrin Lasinger, René Ranftl, Konrad Schindler, and Vladlen Koltun. Towards robust monocular depth estimation: Mixing datasets for zero-shot cross-dataset transfer. *arXiv preprint arXiv:1907.01341*, 2019. 2
- [35] Cheng-Han Lee, Ziwei Liu, Lingyun Wu, and Ping Luo. Maskgan: Towards diverse and interactive facial image manipulation. In *Proceedings of the IEEE/CVF conference on computer vision and pattern recognition*, pages 5549–5558, 2020. 6
- [36] Bo Li, Kaitao Xue, Bin Liu, and Yu-Kun Lai. Bbdm: Image-to-image translation with brownian bridge diffusion models. In *Proceedings of the IEEE/CVF conference on computer vision and pattern recognition*, pages 1952–1961, 2023. 2, 7, 3
- [37] Guan-Hong Liu, Arash Vahdat, De-An Huang, Evangelos A Theodorou, Weili Nie, and Anima Anandkumar. I²sb: Image-to-image schrödinger bridge. *arXiv preprint arXiv:2302.05872*, 2023. 2, 7, 3
- [38] Xingchao Liu and Lemeng Wu. Learning diffusion bridges on constrained domains. In *international conference on learning representations (ICLR)*, 2023. 2
- [39] Xingchao Liu, Lemeng Wu, Mao Ye, and Qiang Liu. Let us build bridges: Understanding and extending diffusion generative models. *arXiv preprint arXiv:2208.14699*, 2022. 2
- [40] Morteza Mardani, Jiaming Song, Jan Kautz, and Arash Vahdat. A variational perspective on solving inverse problems with diffusion models. *arXiv preprint arXiv:2305.04391*, 2023. 2
- [41] Chenlin Meng, Yutong He, Yang Song, Jiaming Song, Jiajun Wu, Jun-Yan Zhu, and Stefano Ermon. Sdedit: Guided image synthesis and editing with stochastic differential equations. *arXiv preprint arXiv:2108.01073*, 2021. 2, 3
- [42] Bernt Oksendal. *Stochastic differential equations: an introduction with applications*. Springer Science & Business Media, 2013. 3
- [43] René Ranftl, Katrin Lasinger, David Hafner, Konrad Schindler, and Vladlen Koltun. Towards robust monocular depth estimation: Mixing datasets for zero-shot cross-dataset transfer. *IEEE transactions on pattern analysis and machine intelligence*, 44(3):1623–1637, 2020. 3
- [44] René Ranftl, Alexey Bochkovskiy, and Vladlen Koltun. Vision transformers for dense prediction. In *Proceedings of the IEEE/CVF international conference on computer vision*, pages 12179–12188, 2021. 2, 3
- [45] Mike Roberts, Jason Ramapuram, Anurag Ranjan, Atulit Kumar, Miguel Angel Bautista, Nathan Paczan, Russ Webb, and Joshua M Susskind. Hypersim: A photorealistic synthetic dataset for holistic indoor scene understanding. In *Proceedings of the IEEE/CVF international conference on computer vision*, pages 10912–10922, 2021. 6
- [46] Robin Rombach, Andreas Blattmann, Dominik Lorenz, Patrick Esser, and Björn Ommer. High-resolution image synthesis with latent diffusion models. In *Proceedings of the IEEE/CVF conference on computer vision and pattern recognition*, pages 10684–10695, 2022. 1, 6
- [47] Chitwan Saharia, William Chan, Huiwen Chang, Chris Lee, Jonathan Ho, Tim Salimans, David Fleet, and Mohammad Norouzi. Palette: Image-to-image diffusion models. In *ACM SIGGRAPH 2022 conference proceedings*, pages 1–10, 2022. 2, 3
- [48] Simo Särkkä and Arno Solin. *Applied stochastic differential equations*. Cambridge University Press, 2019. 3
- [49] Thomas Schops, Johannes L Schonberger, Silvano Galliani, Torsten Sattler, Konrad Schindler, Marc Pollefeys, and Andreas Geiger. A multi-view stereo benchmark with high-resolution images and multi-camera videos. In *Proceedings of the IEEE conference on computer vision and pattern recognition*, pages 3260–3269, 2017. 6
- [50] Yujun Shi, Chuhui Xue, Jun Hao Liew, Jiachun Pan, Han-shu Yan, Wenqing Zhang, Vincent YF Tan, and Song Bai. Dragdiffusion: Harnessing diffusion models for interactive point-based image editing. In *Proceedings of the IEEE/CVF Conference on Computer Vision and Pattern Recognition*, pages 8839–8849, 2024. 2
- [51] Nathan Silberman, Derek Hoiem, Pushmeet Kohli, and Rob Fergus. Indoor segmentation and support inference from rgb-d images. In *Computer Vision—ECCV 2012: 12th European Conference on Computer Vision, Florence, Italy, October 7–13, 2012, Proceedings, Part V 12*, pages 746–760. Springer, 2012. 6
- [52] Jiaming Song, Chenlin Meng, and Stefano Ermon. Denoising diffusion implicit models. *arXiv preprint arXiv:2010.02502*, 2020. 6
- [53] Jiaming Song, Arash Vahdat, Morteza Mardani, and Jan Kautz. Pseudoinverse-guided diffusion models for inverse problems. In *International Conference on Learning Representations*, 2023. 2, 3
- [54] Xuan Su, Jiaming Song, Chenlin Meng, and Stefano Ermon. Dual diffusion implicit bridges for image-to-image translation. *arXiv preprint arXiv:2203.08382*, 2022. 2

- [55] Sxela. <https://github.com/sxela/face2comics>. <https://github.com/Sxela/face2comics>, 2021. 8
- [56] Igor Vasiljevic, Nick Kolkin, Shanyi Zhang, Ruotian Luo, Haochen Wang, Falcon Z Dai, Andrea F Daniele, Mohammadreza Mostajabi, Steven Basart, Matthew R Walter, et al. Diode: A dense indoor and outdoor depth dataset. *arXiv preprint arXiv:1908.00463*, 2019. 6
- [57] Wei Yin, Xinlong Wang, Chunhua Shen, Yifan Liu, Zhi Tian, Songcen Xu, Changming Sun, and Dou Renyin. Diversedepth: Affine-invariant depth prediction using diverse data. *arXiv preprint arXiv:2002.00569*, 2020. 3
- [58] Wei Yin, Jianming Zhang, Oliver Wang, Simon Niklaus, Long Mai, Simon Chen, and Chunhua Shen. Learning to recover 3d scene shape from a single image. In *Proceedings of the IEEE/CVF Conference on Computer Vision and Pattern Recognition*, pages 204–213, 2021. 3
- [59] Conghan Yue, Zhengwei Peng, Junlong Ma, Shiyao Du, Pengxu Wei, and Dongyu Zhang. Image restoration through generalized ornstein-uhlenbeck bridge. *arXiv preprint arXiv:2312.10299*, 2023. 2
- [60] Chi Zhang, Wei Yin, Billz Wang, Gang Yu, Bin Fu, and Chunhua Shen. Hierarchical normalization for robust monocular depth estimation. *Advances in Neural Information Processing Systems*, 35:14128–14139, 2022. 3
- [61] Lvmin Zhang, Anyi Rao, and Maneesh Agrawala. Adding conditional control to text-to-image diffusion models. In *Proceedings of the IEEE/CVF International Conference on Computer Vision*, pages 3836–3847, 2023. 2, 3, 7
- [62] Wenliang Zhao, Yongming Rao, Zuyan Liu, Benlin Liu, Jie Zhou, and Jiwen Lu. Unleashing text-to-image diffusion models for visual perception. In *Proceedings of the IEEE/CVF International Conference on Computer Vision*, pages 5729–5739, 2023. 2
- [63] Linqi Zhou, Aaron Lou, Samar Khanna, and Stefano Ermon. Denoising diffusion bridge models. *arXiv preprint arXiv:2309.16948*, 2023. 2

DPBridge: Latent Diffusion Bridge for Dense Prediction

Supplementary Material

In the supplementary material, we'll provide contents that are not included in the main paper due to page limitations. We first fill in the derivation details of the loss function. Afterwards we will provide the additional quantitative comparisons with more baseline methods. Finally, we will present qualitative examples that apply DPBridge on more dense prediction tasks.

A. Derivation Details

In this section, we'll provide derivation details of the maximum likelihood loss presented in Sec.4.5.1 . Its core is the posterior distribution $q(\mathbf{z}_{t-1}|\mathbf{z}_t, \mathbf{z}_0, \mathbf{z}_T)$ as in Eqn.(5) , whose calculation involves three terms: $q(\mathbf{z}_t|\mathbf{z}_{t-1}, \mathbf{z}_T)$, $q(\mathbf{z}_{t-1}|\mathbf{z}_0, \mathbf{z}_T)$, and $q(\mathbf{z}_t|\mathbf{z}_0, \mathbf{z}_T)$. The last two term of the posterior can be retrieved directly through the marginal distribution of diffusion bridge's forward process, but further derivation is required for the first term. Specifically, as specified in Eqn.(3)

$$\begin{aligned} q(\mathbf{z}_t|\mathbf{z}_0, \mathbf{z}_T) &= \mathcal{N}(m_t\mathbf{z}_0 + n_t\mathbf{z}_T, \sigma_t^2\mathbf{I}) \\ \mathbf{z}_t &= m_t\mathbf{z}_0 + n_t\mathbf{z}_T + \sigma_t\epsilon_t \end{aligned} \quad (14)$$

$$\begin{aligned} q(\mathbf{z}_{t-1}|\mathbf{z}_0, \mathbf{z}_T) &= \mathcal{N}(m_{t-1}\mathbf{z}_0 + n_{t-1}\mathbf{z}_T, \sigma_{t-1}^2\mathbf{I}) \\ \mathbf{z}_{t-1} &= m_{t-1}\mathbf{z}_0 + n_{t-1}\mathbf{z}_T + \sigma_{t-1}\epsilon_{t-1} \end{aligned} \quad (15)$$

To derive the transition probability $q(\mathbf{z}_t|\mathbf{z}_{t-1}, \mathbf{z}_T)$, we substitute \mathbf{z}_0 in Eqn.(14) with derivation from Eqn.(15), obtain

$$\begin{aligned} \mathbf{z}_t &= a_t\mathbf{z}_{t-1} + b_t\mathbf{z}_T + \delta_t\epsilon \\ a_t &= \frac{m_t}{m_{t-1}} \\ b_t &= n_t - \frac{m_t}{m_{t-1}}n_{t-1} = n_t - a_t n_{t-1} \\ \delta_t^2 &= \sigma_t^2 - \frac{m_t}{m_{t-1}}n_{t-1}^2\sigma_{t-1}^2 = \sigma_t^2 - a_t^2\sigma_{t-1}^2 \end{aligned} \quad (16)$$

Thus, we can get $q(\mathbf{z}_t|\mathbf{z}_{t-1}, \mathbf{z}_T) = \mathcal{N}(a_t\mathbf{z}_{t-1} + b_t\mathbf{z}_T, \delta_t^2\mathbf{I})$, which is also a Gaussian distribution.

Putting all these terms back to Eqn.(5) , we'll have:

$$\begin{aligned} & q(\mathbf{z}_{t-1}|\mathbf{z}_t, \mathbf{z}_0, \mathbf{z}_T) \sim \mathcal{N}(\tilde{\boldsymbol{\mu}}_t(\mathbf{z}_t, \mathbf{z}_0, \mathbf{z}_T), \tilde{\sigma}_t^2\mathbf{I}) \\ &= \frac{q(\mathbf{z}_t|\mathbf{z}_{t-1}, \mathbf{z}_T)q(\mathbf{z}_{t-1}|\mathbf{z}_0, \mathbf{z}_T)}{q(\mathbf{z}_t|\mathbf{z}_0, \mathbf{z}_T)} \\ &\propto \exp \left[-\frac{1}{2} \left(\frac{(\mathbf{z}_t - a_t\mathbf{z}_{t-1} - b_t\mathbf{z}_T)^2}{\delta_t^2} + \frac{(\mathbf{z}_{t-1} - m_{t-1}\mathbf{z}_0 - n_{t-1}\mathbf{z}_T)^2}{\sigma_{t-1}^2} - \frac{(\mathbf{z}_t - m_t\mathbf{z}_0 - n_t\mathbf{z}_T)^2}{\sigma_t^2} \right) \right] \\ &= \exp \left[-\frac{1}{2} \left(\left(\frac{a_t^2}{\delta_t^2} + \frac{1}{\sigma_{t-1}^2} \right) \mathbf{z}_{t-1}^2 - 2 \left(\frac{a_t b_t \mathbf{z}_T}{\delta_t^2} + \frac{m_{t-1}\mathbf{z}_0 + n_{t-1}\mathbf{z}_T}{\sigma_{t-1}^2} \right) \mathbf{z}_{t-1} + C(\mathbf{z}_t, \mathbf{z}_0, \mathbf{z}_T) \right) \right]. \end{aligned} \quad (17)$$

where $C(\mathbf{z}_t, \mathbf{z}_0, \mathbf{z}_T)$ indicates the constant term that is independent of \mathbf{z}_{t-1} . Since the Gaussian distribution probability density $\mathbf{z}_{t-1} \sim \mathcal{N}(\tilde{\boldsymbol{\mu}}_t, \tilde{\sigma}_t^2\mathbf{I})$ can be expressed in the following form:

$$\exp \left(-\frac{(\mathbf{z}_{t-1} - \tilde{\boldsymbol{\mu}}_t)^2}{2\tilde{\sigma}_t^2} \right) = \exp \left[-\frac{1}{2} \left(\frac{1}{\tilde{\sigma}_t^2} \mathbf{z}_{t-1}^2 - \frac{2\tilde{\boldsymbol{\mu}}_t}{\tilde{\sigma}_t^2} \mathbf{z}_{t-1} + \frac{\tilde{\boldsymbol{\mu}}_t^2}{\tilde{\sigma}_t^2} \right) \right]. \quad (18)$$

We can thus derive:

$$\begin{aligned} \frac{1}{\tilde{\sigma}_t^2} &= \frac{a_t^2}{\delta_t^2} + \frac{1}{\sigma_{t-1}^2} \\ \Rightarrow \tilde{\sigma}_t^2 &= \frac{\sigma_{t-1}^2(\sigma_t^2 - a_t^2\sigma_{t-1}^2)}{\sigma_t^2} = \frac{\sigma_{t-1}^2}{\sigma_t^2} \delta_t^2 \end{aligned} \quad (19)$$

$$\begin{aligned} \frac{\tilde{\boldsymbol{\mu}}_t}{\tilde{\sigma}_t^2} &= \frac{a_t \mathbf{z}_t - a_t b_t \mathbf{z}_T}{\delta_t^2} + \frac{m_{t-1} \mathbf{z}_0 + n_{t-1} \mathbf{z}_T}{\sigma_{t-1}^2} \\ \Rightarrow \tilde{\boldsymbol{\mu}}_t &= \left[\frac{\sigma_{t-1}^2 (a_t \mathbf{z}_t - a_t b_t \mathbf{z}_T) + \delta_t^2 (m_{t-1} \mathbf{z}_0 + n_{t-1} \mathbf{z}_T)}{\delta_t^2 \sigma_{t-1}^2} \right] \frac{\sigma_{t-1}^2}{\sigma_t^2} \delta_t^2 \\ &= \frac{\sigma_{t-1}^2}{\sigma_t^2} a_t \mathbf{z}_t + \frac{\delta_t^2}{\sigma_t^2} m_{t-1} \mathbf{z}_0 + \left(\frac{\delta_t^2}{\sigma_t^2} n_{t-1} - \frac{\sigma_{t-1}^2}{\sigma_t^2} a_t b_t \right) \mathbf{z}_T \end{aligned} \quad (20)$$

whose results are equivalent to Eqn.(6) and Eqn.(7).

Accordingly, maximizing the Evidence Lower Bound (ELBO) is equivalent to minimizing the KL divergence between ground truth and predicted posterior:

$$\begin{aligned} &KL(q(\mathbf{z}_{t-1} | \mathbf{z}_0, \mathbf{z}_t, \mathbf{z}_T) || p_\theta(\mathbf{z}_{t-1} | \mathbf{z}_t, \mathbf{z}_T)) \\ &= \mathbb{E}_{q(\mathbf{z}_{t-1} | \mathbf{z}_0, \mathbf{z}_t, \mathbf{z}_T)} \left[\log \frac{\frac{1}{\sqrt{2\pi}\tilde{\sigma}_{t-1}} e^{-\frac{(\mathbf{z}_{t-1} - \tilde{\boldsymbol{\mu}}_{t-1})^2}{2\tilde{\sigma}_{t-1}^2}}}{\frac{1}{\sqrt{2\pi}\tilde{\sigma}_{\theta,t-1}} e^{-\frac{(\mathbf{z}_{t-1} - \tilde{\boldsymbol{\mu}}_{\theta,t-1})^2}{2\tilde{\sigma}_{\theta,t-1}^2}}} \right] \\ &= \mathbb{E}_{q(\mathbf{z}_{t-1} | \mathbf{z}_0, \mathbf{z}_t, \mathbf{z}_T)} \left[\log \tilde{\sigma}_{\theta,t-1} - \log \tilde{\sigma}_{t-1} - \frac{(x_{t-1} - \tilde{\boldsymbol{\mu}}_{t-1})^2}{2\tilde{\sigma}_{t-1}^2} + \frac{(x_{t-1} - \tilde{\boldsymbol{\mu}}_{\theta,t-1})^2}{2\tilde{\sigma}_{\theta,t-1}^2} \right] \\ &= \log \frac{\tilde{\sigma}_{\theta,t-1}}{\tilde{\sigma}_{t-1}} - \frac{1}{2} + \frac{\tilde{\sigma}_{t-1}^2}{2\tilde{\sigma}_{\theta,t-1}^2} + \frac{(\tilde{\boldsymbol{\mu}}_{t-1} - \tilde{\boldsymbol{\mu}}_{\theta,t-1})^2}{2\tilde{\sigma}_{\theta,t-1}^2} \end{aligned} \quad (21)$$

If we assume that only the mean term is learnable during training, and $\tilde{\sigma}_{\theta,t-1} = \tilde{\sigma}_{t-1}$, we can ignore all the unlearnable constants and arrive at the final training objective:

$$\begin{aligned} \mathcal{L} &= \mathbb{E}_{t, \mathbf{z}_0, \mathbf{z}_t, \mathbf{z}_T} \left[\frac{1}{2\tilde{\sigma}_t^2} \|\tilde{\boldsymbol{\mu}}_{t-1} - \tilde{\boldsymbol{\mu}}_{\theta,t-1}(\mathbf{z}_t, \mathbf{z}_T, t)\|^2 \right] \\ &= \mathbb{E}_{t, \mathbf{z}_0, \mathbf{z}_t, \mathbf{z}_T} \left[\|\boldsymbol{\epsilon} - \boldsymbol{\epsilon}_\theta(\mathbf{z}_t, \mathbf{z}_T, t)\|^2 \right] \end{aligned} \quad (22)$$

which is the same as in Eqn.(8) and Eqn.(9). This concludes our derivation.

B. Additional Quantitative Results

Next, we provide additional quantitative results on depth estimation (Tab.5) and surface normal prediction (Tab.6) tasks. Compared with Tab.1 and Tab.2 presented in the main paper, we conduct comparisons with more baseline methods, including feed-forward approaches and diffusion-based methods that is trained on more advanced Stable Diffusion (SD) v2.1 backbone. In depth estimation, DPBridge consistently matches state-of-the-art methods, while demonstrating robust generalization across datasets. For example, it achieves 6.9 AbsRel, 95.7 % δ_1 on NYUv2, and 7.5 AbsRel, 94.7% δ_1 on ScanNet. Similarly, for surface normal prediction, DPBridge also delivers competitive results, achieving mean error of 18.1 and 11.25° accuracy of 54.2% on NYUv2, as well as maintaining strong performance on other datasets like iBims-1 (mean: 24.3, 11.25° : 51.2%) and Sintel (mean: 41.2, 11.25° : 19.4%) and. These results highlight DPBridge’s versatility to generalize well across tasks and benchmarks, being comparable to both feed-forward and diffusion-based methods while offering a unified, efficient paradigm to handle dense prediction tasks.

Furthermore, we also evaluate the robustness of DPBridge system by perturbing the input image with different types and different level intensities of noise. The evaluation is conducted under both depth estimation and surface normal prediction tasks. We use NYUv2 and KITTI to report the depth estimation results, as for surface normal prediction, we report the results

Method	Model Type			NYUv2		KITTI		ETH3D		ScanNet		DIODE	
	FF	DM	BM	AbsRel↓	δ_1 ↑								
DiverseDepth [57]	✓			11.7	87.5	19.0	70.4	22.8	69.4	10.9	88.2	37.6	63.1
MiDaS [43]	✓			11.1	88.5	23.6	63.0	18.4	75.2	12.1	84.6	33.2	71.5
LeReS [58]	✓			9.0	91.6	14.9	78.4	17.1	77.7	9.1	91.1	27.1	76.6
Omnidata [19]	✓			7.4	94.5	14.9	83.5	16.6	77.8	7.5	93.2	33.9	74.2
HDN [60]	✓			6.9	94.8	11.5	86.7	12.1	83.3	8.0	93.6	24.6	78.0
DPT [44]	✓			9.8	90.3	10.0	90.1	7.8	94.6	8.2	93.8	18.2	75.8
Marigold* [32]		✓		6.0	95.9	10.5	90.4	7.1	95.1	6.9	94.5	31.0	71.2
DepthFM* [24]		✓		6.5	95.6	8.3	93.4	-	-	-	-	22.5	80.0
Geowizard* [20]		✓		5.7	96.2	14.4	82.0	7.5	94.3	6.1	95.8	31.4	77.1
E2E-FT* [21]		✓		5.4	96.4	9.6	92.1	6.4	95.9	5.8	96.5	30.3	77.6
Marigold [32]		✓		8.6	93.6	13.8	82.6	9.3	93.2	10.4	89.7	33.6	73.9
Geowizard [20]		✓		8.5	93.7	16.2	75.6	9.1	93.1	9.0	93.0	32.0	72.2
E2E-FT [21]		✓		8.2	94.0	15.4	77.9	10.6	89.8	9.2	92.3	32.9	73.7
ControlNet [61]		✓		45.5	54.6	55.2	40.2	30.5	58.8	25.7	68.3	52.1	50.1
InstructPix2Pix [6]		✓		35.2	60.0	47.7	51.2	26.1	66.7	21.4	75.3	44.8	58.0
I2SB [37]			✓	24.9	73.4	37.7	57.9	40.6	52.0	21.2	66.1	40.2	59.1
BBDM [36]			✓	27.9	65.5	47.2	45.1	46.4	48.8	22.7	67.0	34.6	64.7
DPBridge (Ours)			✓	6.9	95.7	11.2	87.3	8.1	93.2	7.5	94.7	29.7	78.6

Table 5. Quantitative comparison of DPBridge with state-of-the-art affine-invariant depth estimation methods on zero-shot benchmarks. All metrics are presented in percentage terms. FF, DM, and BM correspond to feed-forward, diffusion models, and bridge models. The superscript * indicates that this model is trained based on Stable Diffusion v2.1, otherwise is based on Stable Diffusion v1.5.

Method	Model Type			NYUv2		ScanNet		iBims-1		Sintel	
	FF	DM	BM	Mean↓	11.25° ↑	Mean↓	11.25° ↑	Mean↓	11.25° ↑	Mean↓	11.25° ↑
EESNU [3]	✓			16.2	58.6	-	-	20.0	58.5	42.1	11.5
Omnidata v1 [19]	✓			23.1	45.8	22.9	47.4	19.0	62.1	41.5	11.4
Omnidata v2 [31]	✓			17.2	55.5	16.2	60.2	18.2	63.9	40.5	14.7
DSINE [2]	✓			16.4	59.6	16.2	61.0	17.1	67.4	34.9	21.5
Marigold* [32]		✓		18.8	55.9	17.7	58.8	18.4	64.3	39.1	14.9
Geowizard* [20]		✓		19.1	49.5	17.3	53.7	19.5	61.6	40.4	13.2
E2E-FT* [21]		✓		16.5	60.4	14.7	66.1	16.1	69.7	33.5	22.3
Marigold [32]		✓		22.3	40.0	23.3	37.6	28.0	38.5	52.1	8.1
Geowizard [20]		✓		21.7	44.2	22.0	42.1	28.2	37.9	45.8	11.0
E2E-FT [21]		✓		17.7	57.8	17.4	57.4	18.0	64.6	43.9	14.1
DPBridge			✓	18.1	54.2	18.0	54.5	24.3	51.2	41.2	19.4

Table 6. Quantitative comparison of DPBridge with state-of-the-art surface normal prediction methods on zero-shot benchmarks. All metrics are presented in percentage terms. FF, DM, and BM correspond to feed-forward, diffusion models, and bridge models. The superscript * indicates that this model is trained based on Stable Diffusion v2.1, otherwise is based on Stable Diffusion v1.5.

on NYUv2 and iBims-1. Tab. 7 reveals that the model’s performance degrades as noise intensity increases, but the model performance remains acceptable under moderate-level-intensity noise. Among noise types, uniform noise shows the mildest effect on degradation, while salt & pepper and high-intensity gaussian noise cause the most significant performance decline. In addition, the noise intensity has more impact on surface normal prediction than depth estimation, showcasing the inherent characteristics between different tasks. These results emphasize the model’s robustness under moderate noise but still expose its vulnerability to extreme or specific types of noise.

Noise Type	Noise Level	Depth Estimation				Surface Normal Prediction			
		NYUv2		KITTI		NYUv2		iBims-1	
		AbsRel↓	δ_1 ↑	AbsRel↓	δ_1 ↑	Mean↓	11.25° ↑	Mean↓	11.25° ↑
Original Version	-	6.9	95.7	11.2	87.3	18.1	54.2	24.3	51.2
Gaussian	$\mathcal{N}(0, 0.05)$	7.2	94.4	11.8	86.0	18.6	52.2	25.6	45.1
	$\mathcal{N}(0, 0.1)$	8.4	92.7	12.1	85.3	20.3	49.4	27.4	40.4
	$\mathcal{N}(0, 0.2)$	10.3	90.0	15.7	78.6	24.6	43.7	37.0	25.4
	$\mathcal{N}(0, 0.5)$	15.9	77.2	22.5	67.1	41.3	22.5	50.0	13.2
Uniform	$\mathcal{U}(-0.05, 0.05)$	7.0	95.0	11.4	86.5	18.3	53.6	24.5	50.7
	$\mathcal{U}(-0.1, 0.1)$	7.2	94.7	11.5	85.4	18.7	53.0	24.8	49.4
	$\mathcal{U}(-0.2, 0.2)$	7.6	94.0	12.0	85.0	19.5	50.5	26.0	46.1
	$\mathcal{U}(-0.5, 0.5)$	9.3	91.1	16.3	76.1	22.4	42.2	30.2	31.6
Poisson	<i>Poisson</i> ($\lambda = 0.05$)	10.2	90.2	13.1	82.5	21.3	45.6	28.1	38.9
	<i>Poisson</i> ($\lambda = 0.1$)	11.8	88.9	15.4	79.3	23.2	40.3	34.9	24.8
Salt & Pepper	<i>Probability=5%</i>	12.0	85.4	13.3	81.7	26.3	28.8	31.8	29.6
	<i>Probability=10%</i>	14.3	82.2	16.0	76.2	28.6	26.3	35.3	21.4

Table 7. Robustness evaluation on depth estimation and surface normal prediction tasks with different types and different intensities of noise. During all experiments, the input images are normalized between -1 to 1.

C. Additional Qualitative Results

To further validate the effectiveness and generalization of DPBridge, we provide qualitative results for various dense prediction tasks, including semantic segmentation, optical flow prediction, and style transfer, by framing them as continuous-valued image-to-image translation problems. For semantic segmentation, we convert discrete labels into color maps and use our bridge model to predict colors in RGB space instead of categorical labels. For optical flow, the bridge process is defined between the flow image and the first image in the input RGB pair. To accommodate this, we adapt the UNet architecture to incorporate both RGB images as conditions during inference and convert the flow map into RGB space, predicting corresponding colors rather than uv coordinates. The following figures (Fig.5, Fig.6, Fig.7, Fig.8) illustrate that DPBridge achieves visually satisfactory results across different tasks. Note that only qualitative assessments are presented here; detailed implementations and quantitative evaluations are left as directions for future research.

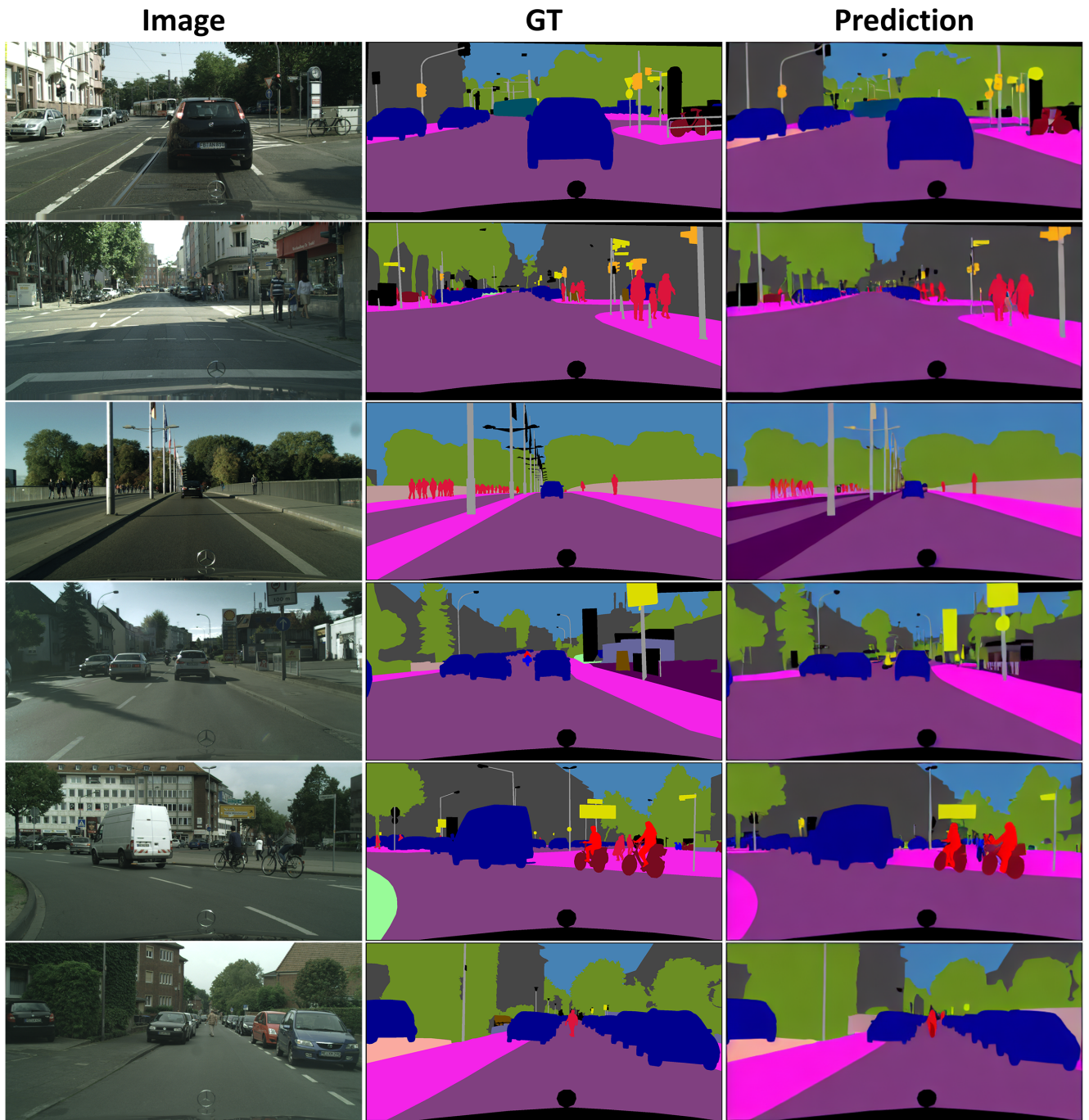


Figure 5. Qualitative examples of applying DPBridge to semantic segmentation task on CityScape [14] dataset. We transform discrete labels into color maps and use our bridge model to predict colors in RGB space instead of categorical labels.

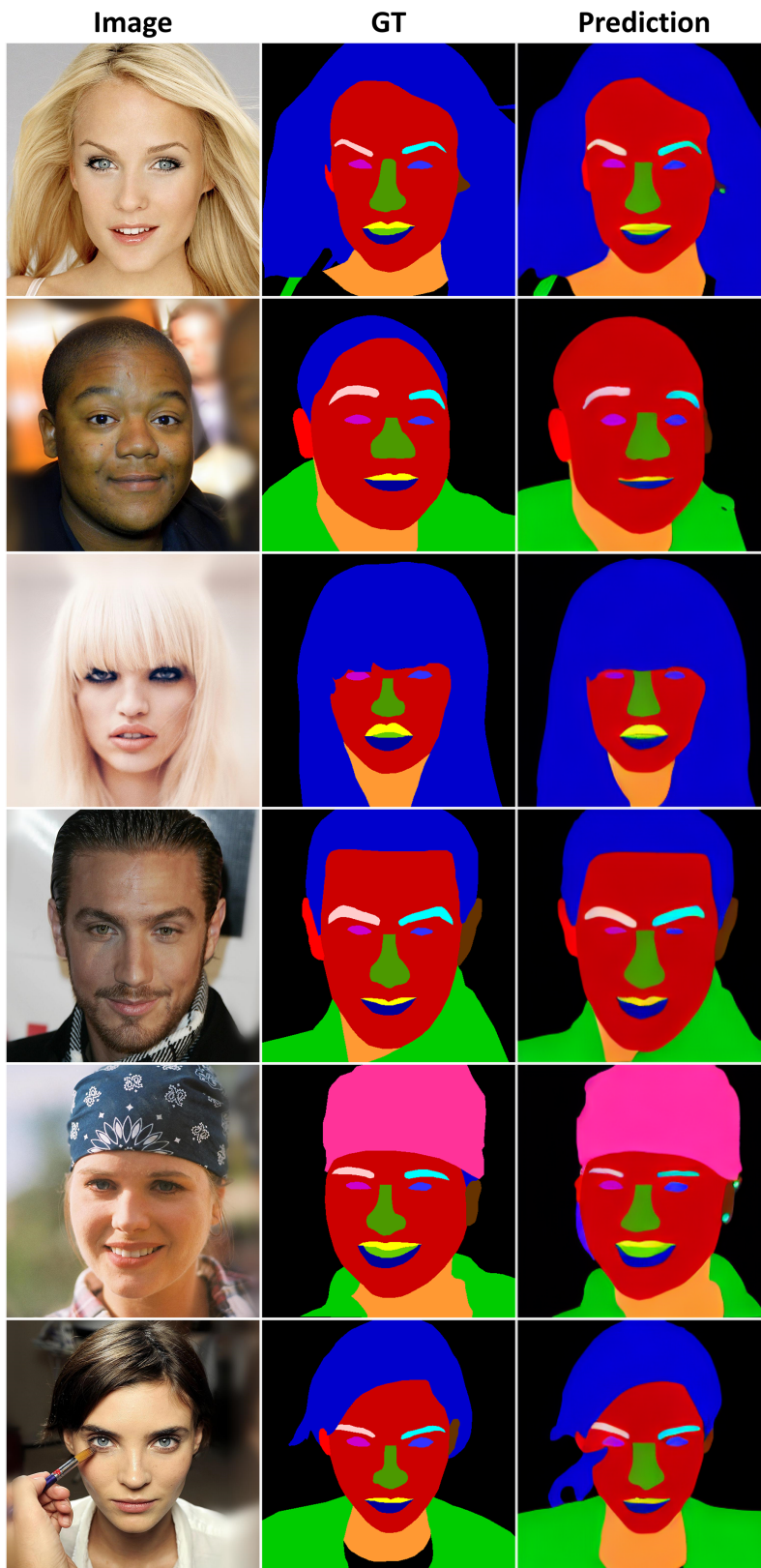


Figure 6. Qualitative examples of applying DPBridge to semantic segmentation task on CelebAMask-HQ [35] dataset. We transform discrete labels into color maps and use our bridge model to predict colors in RGB space instead of categorical labels.

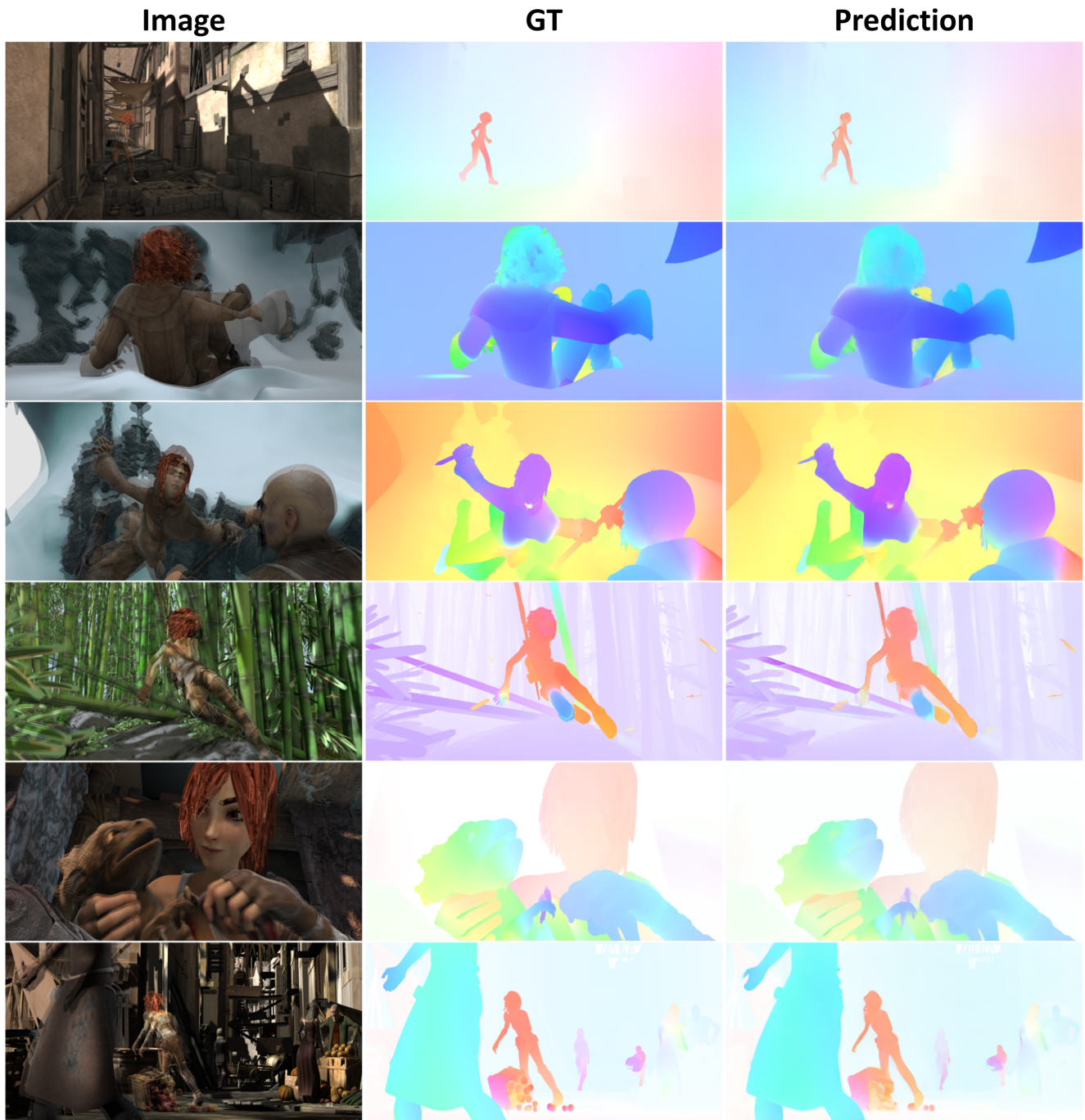


Figure 7. Qualitative examples of applying DPBridge to optical flow prediction task on MPI-Sintel [7] dataset. The input image is the overlaid RGB pair, and we transform the flow map into RGB space so that the diffusion bridge process can be constructed accordingly.

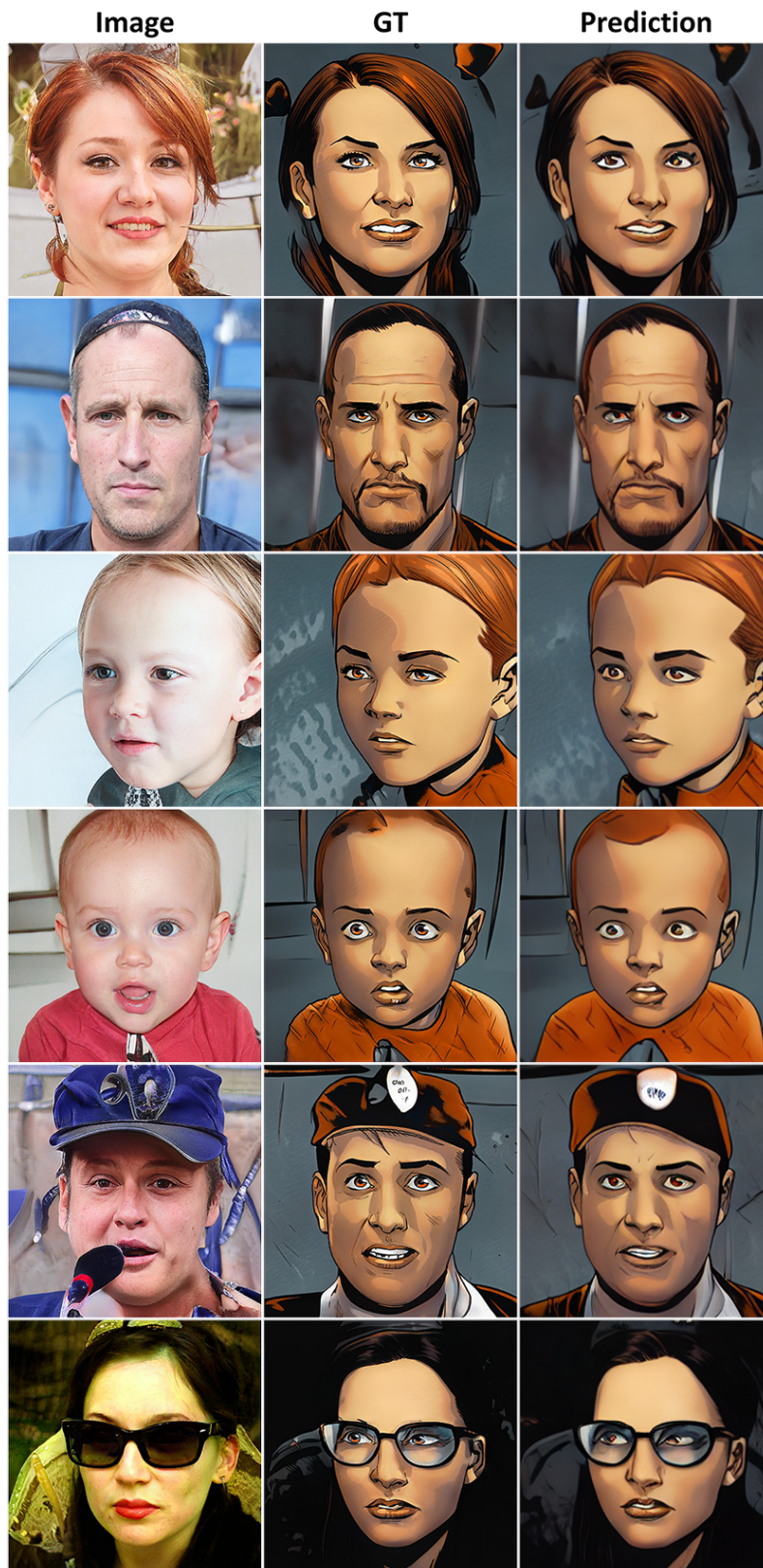


Figure 8. Qualitative examples of applying DPBridge to style transfer task on Face-to-Comics [55] dataset.